CRYSTAL GROWTH & DESIGN

Article

pubs.acs.org/crystal

The Effects of Inorganic Additives on the Nucleation and Growth Kinetics of Calcium Sulfate Dihydrate Crystals

Taher Rabizadeh,*[,†] Tomasz M. Stawski,[†,‡] David J. Morgan,[§] Caroline L. Peacock,[†] and Liane G. Benning*[,†,‡,∥]

[†]Cohen Geochemistry Laboratory, School of Earth and Environment, University of Leeds, Leeds, LS2 9JT, United Kingdom

[‡]GFZ, German Research Centre for Geosciences, Telegrafenberg, 14473 Potsdam, Germany

[§]Cardiff Catalysis Institute, School of Chemistry, Cardiff University, Cardiff, CF10 3AT, United Kingdom

[∥]Department of Earth Sciences, Free University of Berlin, 12249 Berlin, Germany

Supporting Information

ABSTRACT: The effects that 50−500 mM aqueous Li^+, Na^+, K^+, and Mg^{2+} have on the crystallization kinetics of calcium sulfate dihydrate (gypsum; $CaSO_4{\cdot}2H_2O$) were determined by *in situ* and time-resolved UV−vis spectrophotometry. The mechanisms of surface or structural associations between these additives and the end-product gypsum crystals were evaluated through a combination of inductively coupled plasma mass and/or optical emission spectrometric analyses of digested end-products and X-ray photoelectron spectroscopy of the surface of the solids. Furthermore, X-ray diffraction and scanning electron microscopy were utilized for determining any changes in phase composition and growth morphologies of the formed crystals. Our results revealed that Mg^{2+}, even at low concentrations, decreased the nucleation and growth kinetics 5−10 fold more than Li^+, Na^+, and K^+. In all cases, the additives also changed the shapes and sizes of the formed crystals, with Mg^{2+} and Li^+ resulting in longer and narrower crystals compared to the additive-free system. In addition, we show that, regardless of concentration, Mg^{2+}, Li^+, and K^+ only adsorb to the newly forming surfaces of the growing gypsum crystals, while ∼25% of Na^+ becomes incorporated into the synthesized crystals.

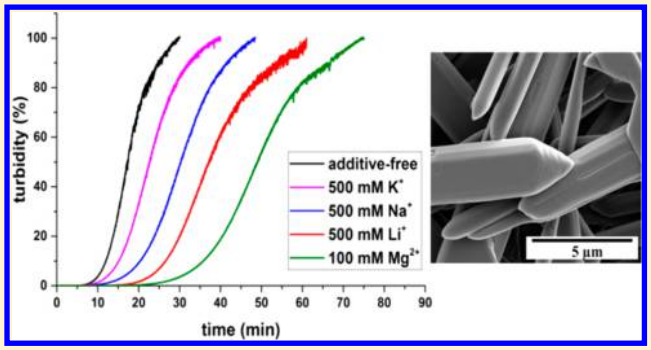

1. INTRODUCTION

Gypsum is one of the main evaporitic minerals forming at Earth surface conditions.[1] In addition, gypsum is a crucial mineral extensively used in various industries for construction, medical, or agricultural applications.[2−4] However, in several industrial processes that rely on water handling systems (e.g., oil and gas production, water desalination), the precipitation of gypsum results in its deposition as mineral scales on pipes, filters, and heat exchangers.[5−7] This leads to increased cost and reduction in production efficiency. Thus, it is paramount to quantitatively understand how gypsum forms in such systems. Particularly, the effects that aqueous ions present in, for example, formation waters may have on the crystallization kinetics and morphology of gypsum are still poorly understood.

It is well-known that both inorganic[8,9] and organic additives[10,11] affect the nucleation, crystallization, and morphologies of gypsum crystals. To date, primarily the role that elements like Cr^{3+}, Cu^{3+}, Cr^{6+}, Al^{3+}, and Fe^{3+} have on gypsum growth from solution have been studied.[12−15] In contrast, a mechanistic understanding of the effect that major ions in, for example, brines or formation waters (e.g., Na^+, K^+, Li^+, Cl^-, or Mg^{2+}) has on gypsum crystallization is still lacking. Existing data from studies that address the crystallization of calcium sulfate phases in the presence of these ions are highly discrepant, and whether these ions become structurally incorporated or only surface adsorbed into the growing gypsum is still debated. For example, Na^+ has been shown to incorporate into the calcium sulfate hemihydrate ($CaSO_4{\cdot}0.5H_2O$; bassanite)[16] but not into gypsum.[17] On the other hand, Mg^{2+} was suggested to only incorporate into gypsum.[17] However, lacking so far is a quantitative and molecular level understanding of the processes that lead to these ions becoming either adsorbed onto or incorporated into growing gypsum crystal structures. Lacking is also a mechanistic pathway explaining the role that these crucial ions in brines have on the crystallization of gypsum.

To fill this gap, we have in this work elucidated the effects of aqueous Li^+, Na^+, K^+, and Mg^{2+} ions on the nucleation and growth kinetics, as well as the morphology of gypsum crystals forming from supersaturated aqueous solutions. We followed the processes by combining analyses of the solution and solid end-products and determined the mechanisms that control the

Received: September 29, 2016
Revised: December 18, 2016
Published: December 20, 2016

DOI: 10.1021/acs.cgd.6b01441
Cryst. Growth Des. 2017, 17, 582−589

way these alkali and alkaline earth cations became associated with growing gypsum crystals. We show, in contrast to previous studies, that Li^+, K^+, and Mg^{2+} do not incorporate into the gypsum structures, while ~25% of Na^+ becomes incorporated. However, the major effect that all ions have is in delaying the nucleation and growth through adsorption onto the growing mineral surfaces. In the case of Mg^{2+} and Li^+, this interaction also leads to a change in the resulting crystal growth morphologies.

2. EXPERIMENTAL METHODS

Calcium and sulfate stock solutions were prepared from dissolving analytical grade $CaCl_2{\cdot}2H_2O$ (≥99−100%; AnalaR Normapour; VWR) and diluting concentrated H_2SO_4 (93−98% v/vol, AnalaR Normapour; VWR) in 18 MΩ cm^{-1} ultrapure Milli-Q water to reach concentrations of 200 mM. The effects of inorganic metal ions on gypsum crystallization were evaluated by adding Li^+, Na^+, K^+, and Mg^{2+} to separate $CaCl_2{\cdot}2H_2O$ stock solutions, using analytical grade LiCl (puriss. p.a., anhydrous, ≥99.0%; Sigma-Aldrich), NaCl (≥99.9%; Fisher), KCl (puriss. p.a., anhydrous, ≥99−100%; Sigma-Aldrich), and $MgCl_2{\cdot}6H_2O$ (≥99−100%; AnalaR Normapour; VWR). Precipitates were produced by mixing 1 mL of $CaCl_2{\cdot}2H_2O$ with or without the additives with 1 mL of H_2SO_4 in 4 mL of polystyrene cuvettes at room temperature (21 °C) and under constant stirring. The mixing led to a solution with a pH of ~2 and initial Ca^{2+} and SO_4^{2-} concentrations of 100 mM. The initial concentration of additives in the crystallization solutions (after mixing) was varied between 50 and 500 mM. Once mixed, all solutions were supersaturated with respect to gypsum as indicated by the saturation indices (as the logarithm of the ion activity product over the solubility product) calculated with the geochemical computer code PhreeqC 3.3.3 and using the PITZER database.[18]

Changes in the mixed solutions were monitored by measuring the increase in absorbance using a UV−vis spectrophotometer (Uvikon XL) at λ = 520 nm with an angle between the incident beam and detector of 180°. The reactions were followed at room temperature for up to 200 min with UV−vis data collected every second, and each experimental set was carried out five times. The absorbance data are plotted as the normalized change in solution turbidity. At the end of each turbidity experiment, the contents of each cuvette were vacuum filtered through 0.2 μm polycarbonate filters, dried, and preserved for further analyses (for additional details, see the Supporting Information; Figure S1).

In all experiments, regardless if additives were present or not, the solid end-products were always gypsum as determined by powder X-ray diffraction (XRD; Bruker D8 diffractometer; Cu Kα_1; 2θ range 5−35°; resolution 0.105°/step; counting time 1 s/step) with XRD patterns analyzed with the EVA software (version 3) and the PDF-2-1996 database (see Figure S2). To accurately determine the d-spacing in all samples, each gypsum end-product powder was mixed with a silicon standard reference material prior to the XRD analysis.

The growth morphologies (different from equilibrium morphologies[19]) of the resulting gypsum crystals were imaged using a field emission gun scanning electron microscope (FEG-SEM, FEI Quanta 650, 5 kV), and the dimensions of the crystals were evaluated by measuring the lengths and widths of 200 crystals in each sample using the ImageJ v. 1.49 software.[20]

To evaluate the association between the additives and the formed gypsum, aliquots of the precipitated end-products were dissolved in 2% nitric acid (69% AnalaR NORMAPUR analytical reagent) and the resulting solutions were analyzed for their Li^+, Na^+, K^+, Mg^{2+}, and Ca^{2+} contents by inductively coupled plasma mass spectrometry (ICP-MS; Thermo Scientific iCAPQc) and inductively coupled plasma optical emission spectrometry (ICP-OES; Thermo Scientific iCAP 7400); for limit of detection and uncertainties, see Table S1. To differentiate between the potentially surface adsorbed and the structurally incorporated fractions of the additives, in each case, a 0.5 g aliquot of an end-product gypsum sample was suspended in 25 mL of a saturated gypsum solution and filtered. Subsequently, the gypsum on filter was then filter-rinsed 6 times with 25 mL of saturated gypsum solutions (total rinsing time of ~10 min) to desorb any potentially surface adsorbed additives. The saturated gypsum solution was prepared by equilibrating gypsum (puriss, 99.0−101.0%, Sigma-Aldrich) in 18 MΩ cm^{-1} ultrapure Milli-Q water at pH 2 for 24 h and filtering through 0.2 μm syringe filters prior to desorption. After this desorption step, the remaining solids were digested in 2% nitric acid and the digestion solutions were analyzed as described above. The concentrations of additives associated with the end-product gypsum crystals (association amount; C_A) before and after desorption were calculated from the moles of cation measured in the full digestion solution divided by the moles of total dissolved gypsum crystals.

Finally, to determine the nature of the surface interactions between the various ions and the formed precipitates, we employed X-ray photoelectron spectroscopy (XPS) with a detection limit of 0.1 at. % (which is roughly 1 ppth or 10^{19} atoms/cm^3). On both the as-formed and the desorbed end-product solids, XPS was used to determine whether and how additives were associated with the mineral surfaces or the crystal structures. XPS spectra were acquired from the top 8−10 nm of end-product gypsum crystals using a Kratos Axis Ultra-DLD spectrometer with a monochromatic Al Kα X-ray source (144 W) and analyzer pass energies of either 160 eV (survey scans) or 40 eV (high resolution scans). The base pressure during analysis was ca. 6×10^{-7} Pa. All data were referenced to the C (1s) signal of adventitious carbon at 284.8 eV and quantified as atomic percentage using CasaXPS (Version 2.3.15) using elemental sensitivity factors supplied by the manufacturer.

3. RESULTS

3.1. The Effects of Additives on the Crystallization Process. In the additive-free experiments, the turbidity started to develop after 3 ± 1 min (induction time) and it took ~30 min for the turbidity to reach a steady value on a plateau (Figure 1a). In contrast, in each of the additive-containing experiments (Figure 1a,b), the induction times and the time to reach a plateau were markedly longer. At the highest concentration (500 mM) of monovalent cations (Li^+, Na^+, and K^+), the induction time increased in the order of K^+ < Na^+ < Li^+ by 2-fold, 4-fold, and almost 5-fold, respectively (Table S2). The slope of the turbidity decreased and the crystallization end-plateaus were reached significantly later than in the additive-free system in the same order (K^+ ~ 37 min, Na^+ ~ 48 min, and Li^+ ~ 60 min; Figure 1a). The turbidity development was even more affected by the presence of Mg^{2+}. Even at a low additive concentration (e.g., 100 mM; Figure 1a), the induction time was much longer than for all monovalent cations at 500 mM. Quadrupling the Mg^{2+} concentration from 50 to 200 mM increased the induction time exponentially (Figure 1b, Table S2). Furthermore, for Mg^{2+} at 300 and 500 mM even after 200 min of reaction, no change in turbidity was observed, indicating total inhibition of the reaction under these experimental conditions. For all additives with increasing cation concentrations, the induction time increased linearly (Figure 1c), but the effect was markedly larger for the divalent Mg^{2+} compared to the monovalent Li^+, Na^+, and K^+ (Figure 1c).

3.2. The Association between Additives and Gypsum Crystals. For all additive ions, increasing additive concentration in solution was mirrored by an increase in associated ion concentration (C_A) in the solids formed (Figure 2a−d). For example, for monovalent additive concentrations between 50 and 500 mM, C_{A,Li^+} increased ~5 times, while C_{A,Na^+} and C_{A,K^+} increased ~4 and ~3 times, respectively (Figure 2a−c). For Mg^{2+} at concentrations up to 200 mM, the $C_{A,Mg^{2+}}$ increased ~4 times (Figure 2d) and reached a value almost equivalent to the

DOI: 10.1021/acs.cgd.6b01441
Cryst. Growth Des. 2017, 17, 582−589

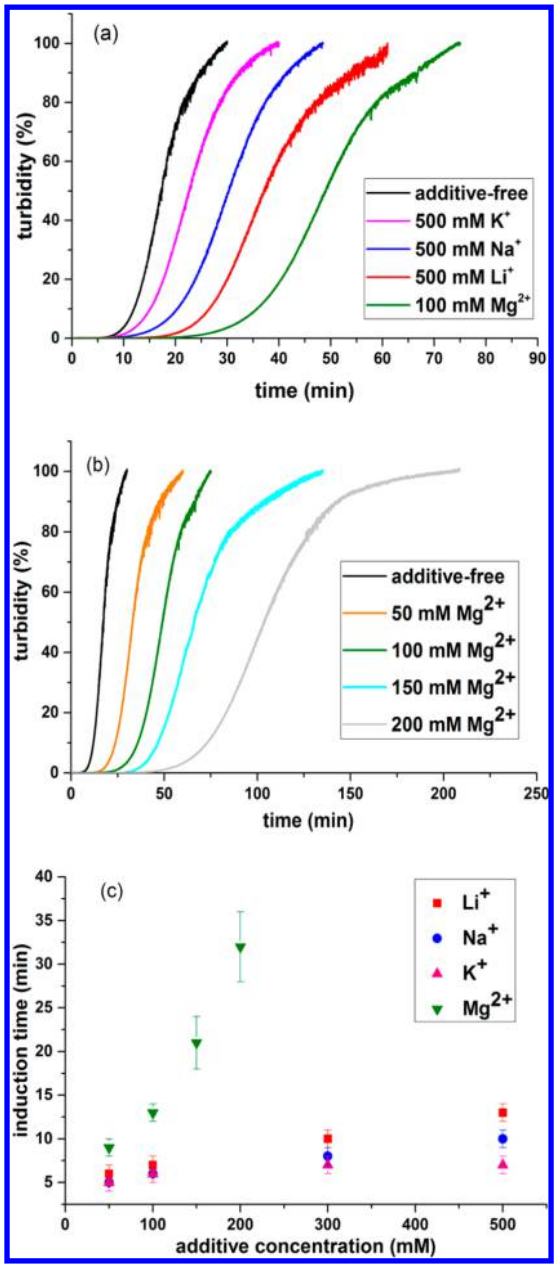

Figure 1. Turbidity curves plotted as a function of time (a) in the absence and presence of high concentrations of additives (note that Mg^{2+} is only 100 mM, while all monovalent ions are 500 mM) and (b) at variable concentrations of Mg^{2+}. (c) Changes in induction times as a function of additive concentrations.

highest value obtained for the C_A of Li^+ at 500 mM. Comparing the association amounts at a fixed additive concentration (100 mM), mirrors the trend observed for the increase in induction time, namely, $K^+ < Na^+ < Li^+ < Mg^{2+}$.

When we evaluated the partitioning of additives between crystal surfaces (adsorption) or crystal matrixes (structural incorporation), our data revealed that the C_A for Li^+, K^+, and Mg^{2+} in the postdesorption digested samples were below detection limits. This clearly indicated that these cations were only adsorbed to the surfaces of the growing gypsum crystals with insignificant or no incorporation into the crystal structures. In contrast, at the highest additive concentrations (500 mM), up to 25% of the associated Na^+ ($C_{A,500\ mM}$ = 0.002 out of 0.009) became incorporated into the gypsum structure (Figure

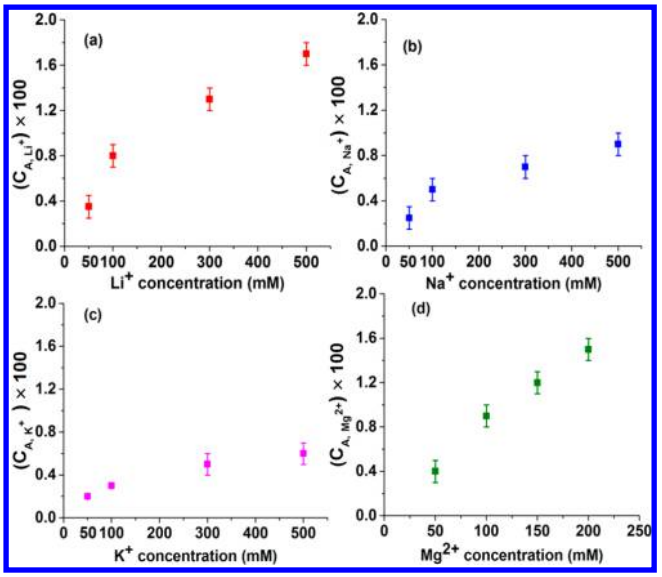

Figure 2. Variations in cation association at different concentrations of (a) Li^+, (b) Na^+, (c) K^+, (d) Mg^{2+}; the error bars represent the standard deviations measured in five replicate samples.

S3). The additive ion adsorption was also confirmed by XPS surface analyses of as-formed and desorbed gypsum crystals (Figure 3). The XPS spectra confirmed that the Li 1s (55.8 eV), K $2p_{3/2}$ (292.9 eV), and Mg 2s (89.8 eV) peaks were present in all as-formed samples but absent in the postdesorbed ones, confirming that these ions were solely surface adsorbed and not incorporated into the gypsum structure (Figure 3a,c,d). On the other hand, for Na^+, the 1s peak at 1071.6 eV was present in both the as-formed and desorbed gypsum spectra, again corroborating our C_A data (Figure 3b) that a fraction of the associated Na^+ became sequestered into the gypsum crystal structure. The surface elemental compositions (in atomic percentage) of the as-produced and desorbed gypsum crystals illustrated that Li^+ had the highest adsorption affinity (1.5 at. %), followed by Mg^{2+} (1.1 at. %), Na^+ (0.4 at. %), and K^+ (0.4 at. %) (Table 1). However, unlike Li^+, K^+, and Mg^{2+}, Na^+ remained associated with the gypsum crystals postdesorption (0.1 at. %), confirming its structural incorporation. Note that the signal of lithium is low due to its small ionization cross section and in part covered by the large satellite peak visible in Figure 3.

Together with the adsorbed ions, in all as-formed but not the desorbed samples, the XPS spectra revealed the presence of Cl^- $2p_{3/2}$ peaks, confirming that Cl^- also became coadsorbed to the gypsum surfaces (Figure S4). Furthermore, the Ca to S atomic % ratio was close to 1:1 but the O to Ca or S ratio was higher than 4:1, likely related to gypsum structural water (Table 1).

3.3. The Effects of Additives on the Morphology of Gypsum. Micrographs of the formed gypsum crystals revealed that, in the additive-free system, short (4−6 μm) and narrow (2−2.5 μm) gypsum crystals formed (Figures 4a, 5a,b, and S6a,b). In contrast, the crystals from the additive-containing solutions were markedly longer and narrower (Figures 4b, 5b, and S6a,b). For example, in the presence of 500 mM Li^+, the end-product gypsum crystals were ∼200% longer and ∼50% narrower compared with the additive-free crystals.

This is clearly visible that, in the presence of Li^+ and Mg^{2+}, the length of the resulting crystals almost doubled, while the

DOI: 10.1021/acs.cgd.6b01441
Cryst. Growth Des. 2017, 17, 582−589

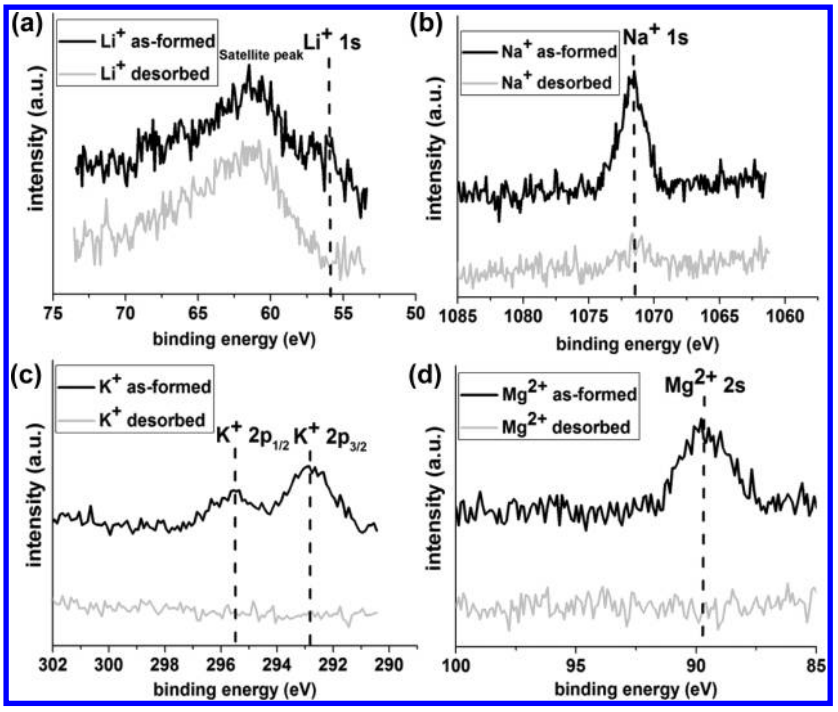

Figure 3. XPS spectra for the as-formed and desorbed gypsum crystals containing additive cations. Note that the peak intensities are in arbitrary units and do not represent the concentration of the elements on the surface.

Table 1. Surface Composition of the Precipitated Gypsum Crystals Detected by XPS (at. %)

	Ca	S	O	Li	Na	K	Mg	Cl	C[a]
additive-free (as-formed)	11.5	12.0	58.3						18.2
additive-free (desorbed)	11.6	12.0	58.3						18.1
Li^+-500 mM (as-formed)	9.6	10.0	52.3	1.5				1.7	24.9
Li^+-500 mM (desorbed)	12.0	12.7	57.3						18.0
Na^+-500 mM (as-formed)	12.6	13.1	59.5		0.5			0.1	14.2
Na^+-500 mM (desorbed)	12.3	13.0	59.4		0.1				15.2
K^+-500 mM (as-formed)	12.2	12.7	58.8			0.4		0.1	15.8
K^+-500 mM (desorbed)	12.3	13.1	59.9						14.7
Mg^{2+}-200 mM (as-formed)	10.2	10.9	48.9				1.1	1	27.9
Mg^{2+}-200 mM (desorbed)	12.3	12.9	57.9						16.9

[a]Adventitious carbon.

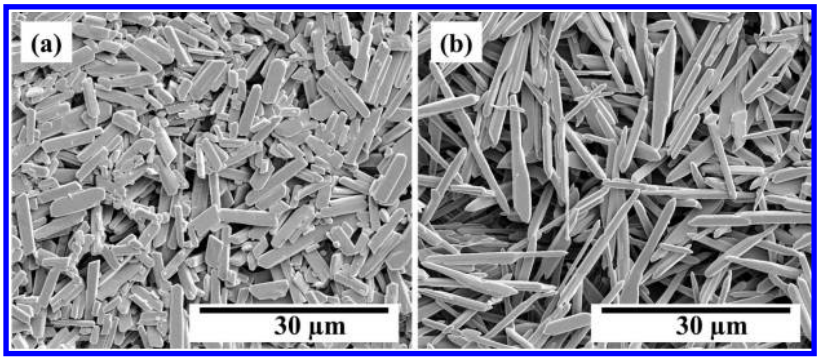

Figure 4. SEM micrographs of the end-product gypsum crystals in (a) the additive-free system and in (b) the presence of 500 mM Li^+ (for morphologies of gypsum crystals precipitated in the presence of K^+, Na^+, and Mg^{2+}, see Figure S5).

width slightly decreased compared to the additive-free system (Figures 5a,b and S6a,b).

In addition, the tips of the growing gypsum crystals differed (Figures 6a–e and S7–S10), with the additive-free crystals having dominantly flat tips. For example, in the presence of Li^+, the tips were broader and thicker and, in these crystals, small spiral growth steps were visible (e.g., Figures 6b and S7c). Similarly, the gypsum crystals precipitated in the presence of 500 mM Na^+ (Figure S8) and K^+ (Figure S9) had uneven tips also with small steps, while the Mg^{2+} modified gypsum crystals had curved tips (Figures 6e and S10).

DOI: 10.1021/acs.cgd.6b01441
Cryst. Growth Des. 2017, 17, 582–589

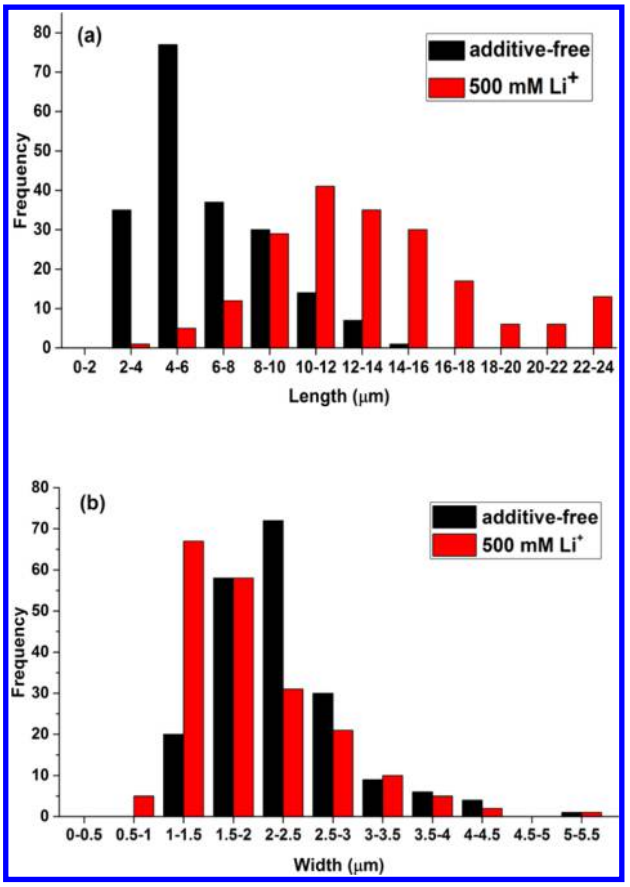

Figure 5. Particle size analysis of gypsum crystals precipitated from solution containing 500 mM Li^+ after 200 min: (a) length of the crystals; (b) width of the crystals (the particles size analysis of the gypsum crystals precipitated in the presence of 500 mM K^+, 500 mM Na^+, and 200 mM Mg^{2+} are in Figure S6a,b).

4. DISCUSSION

4.1. Crystallization Kinetics: Role of Additives. We used the change in turbidity induction times in the absence and presence of the additives as a proxy to evaluate the effects they have on the nucleation and growth of gypsum. Our data showed a clear increase in induction time with increasing additive concentrations, and a decrease in nucleation and growth kinetics in the order of $K^+ < Na^+ < Li^+ < Mg^{2+}$ (Figure 1a–c). To fully understand the interaction, we also assessed how the crystallization process (i.e., nucleation and growth) was affected by the presence of the additives.

The increase in ionic strength (IS) with increasing the additive concentrations from 50 to 500 mM invariably resulted in a decrease in the activities of SO_4^{2-} and Ca^{2+}, and this affected the solubility of gypsum and delayed its precipitation (Figure 1a–c). This is a well-known process in the $CaSO_4$ system.[21−24] Specially, at high ion concentrations, and thus high ionic strengths (IS = 1 and 1.1 M for 500 mM monovalent cations and 200 mM Mg^{2+} containing solutions, respectively), additives can be present as ion pairs or charged complexes.[25] Such complexes further decrease the activity of free SO_4^{2-} and $CaSO_4^0$ ion pairs. In our study, the additive−sulfate ion-paring strength increased in the order of $K^+ < Na^+ < Li^+ < Mg^{2+}$ ($[KSO_4]^- < [NaSO_4]^- < [LiSO_4]^- < [MgSO_4^0]$).[25−28] As such, this likely explains our observation that Mg^{2+} decreased the nucleation rate and increased the solubility of the gypsum crystals more than the monovalent cations. However, it is important to note that the observed order in which these ions affected the induction time and crystallization kinetics ($K^+ < Na^+ < Li^+ < Mg^{2+}$) is different to what was predicted from the saturation indices calculated by PhreeqC ($Na^+ < Li^+ < K^+ < Mg^{2+}$; Table S3).

Once nucleation is overcome, most often the rate-limiting step for crystal growth is determined by cation desolvation.[29] The increase in hydration enthalpy for $K^+ < Na^+ < Li^+ < Mg^{2+}$ reveals that, in our system, the divalent Mg^{2+} ion with the highest hydration enthalpy and water residence time[30] by far outcompetes the monovalent ions as it limits crystal growth more effectively. Among the monovalent ions, Li^+ retained its water longer than Na^+ and K^+.[31]

This is similar to the inhibitory order for the precipitation of calcium oxalate monohydrate[32] or for barium sulfate.[33]

4.2. Surface Adsorption and/or Structural Incorporation. Our results (Figures 2, 3, and S3) revealed that all the tested inorganic additives adsorbed onto the surfaces of the gypsum crystals and that, among them, the cations with more negative hydration enthalpies (Li^+ and Mg^{2+}) had the highest surface adsorption affinity (Table 1). This behavior can be explained by the water "structure making-structure breaking" model.[34] According to this model, an ion and a surface exerting similar structural effects on their surrounding water are attracted entropically to each other. Gypsum has a negative heat of hydration[35] and retains H_2O molecules in the vicinity of its surface and fits, therefore, to the structure-making model. These H_2O molecules may thus act as anchoring points for the stronger adsorption of Li^+ and Mg^{2+}, which are structure-making ions compared to Na^+ and K^+. In addition, equivalent adsorption (in atomic percentage) of Mg^{2+} and Li^+ (Table 1) despite the more than 2-fold lower concentration of Mg^{2+} (200 mM) than Li^+ (500 mM) further supports this mechanism. Similar behaviors (i.e., higher surface adsorption of Li^+ than Na^+ and K^+) have been reported for TiO_2[36] and α-Al_2O_3.[37]

Our data (Table 1 and Figure S4) also showed a high adsorption affinity of Cl^- on the as-formed gypsum crystals precipitated in the presence of Li^+ and Mg^{2+} but only a trace amount of Cl^- on the gypsum crystals formed in the presence of Na^+ and K^+. Sakuma and Kawamura[38] used molecular dynamics modeling and suggested that cations coadsorbed with chloride on muscovite surfaces. In addition, Rahnemaie et al.[39] documented that, in the goethite-solution double layer, Cl^- was closer to the surface than the other ions, and that Li^+ and Na^+ were at the intermediate position of the double layer and K^+ was at the largest distance.

Our observations are in agreement with these previous reports for the monovalent ions Li^+, Na^+, and K^+, but we evidenced further the role of Li^+ and Mg^{2+} in coadsorbing the chloride ion. This is further supported by the fact that neither on the surfaces of the as-formed additive-free gypsum crystals nor in all the postdesorption gypsum crystals was Cl^- detected by XPS (Table 1 and Figure S4). This was despite the fact that, in all initial solutions used for precipitating gypsum crystals in these additive-free experiments, calcium chloride was the major source of Cl^- (200 mM). Moreover, in the samples where Li^+ and Mg^{2+} ions and chloride were determined to be adsorbed to the gypsum surfaces (Table 1), the atomic percentage of the adsorbed Cl^- was in a ratio close to 1:1 with the adsorbed Li^+ and Mg^{2+}. This suggest that Li^+ and Mg^{2+} likely adsorbed onto the gypsum surfaces as chloride ion pairs or complexes such as $LiCl(H_2O)_4$ for Li^+ and $[MgCl(H_2O)_M]^+$ for Mg^{2+}.[40,41] For Li^+, this is supported by the fact that the binding energies for Li 1s

DOI: 10.1021/acs.cgd.6b01441
Cryst. Growth Des. 2017, 17, 582−589

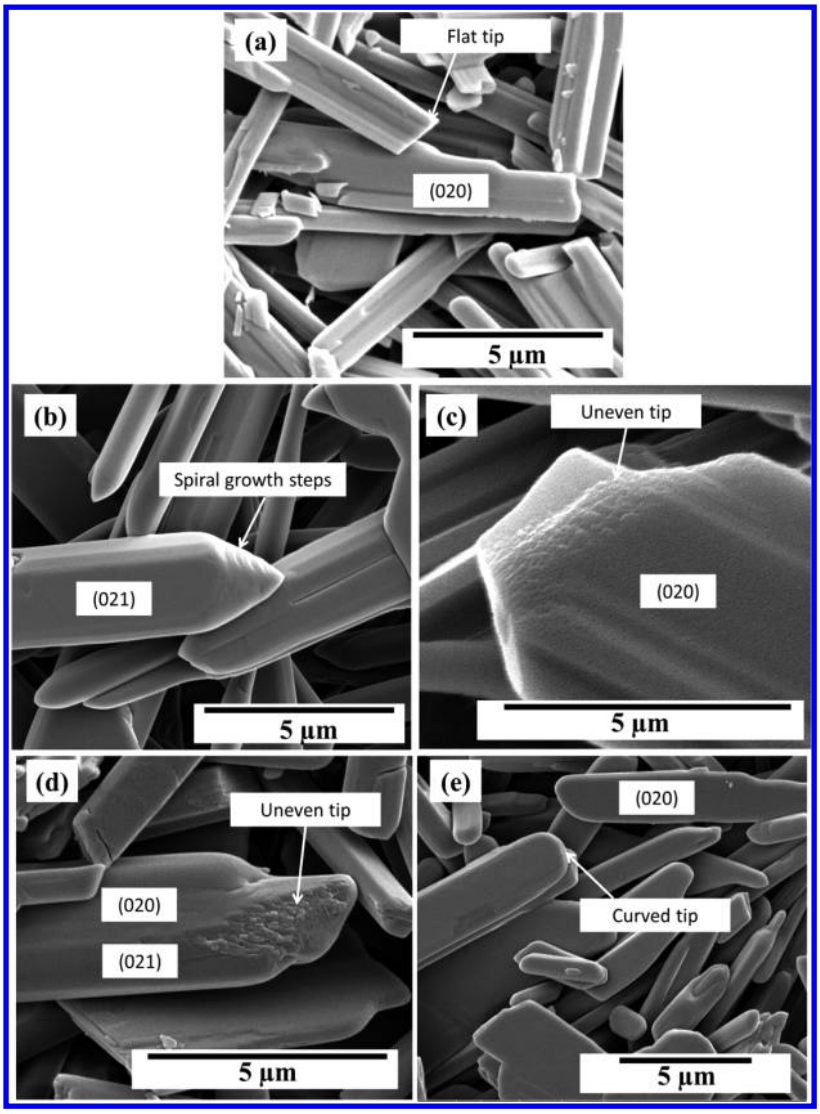

Figure 6. SEM micrographs of end-product gypsum tips from systems with (a) no additive, (b) 500 mM Li^+, (c) 500 mM Na^+, (d) 500 mM K^+, and (e) 200 mM Mg^{2+}. Note that indexed faces of the crystals formed in the presence of the additives are tentatively assigned, because round shapes are difficult to index based on SEM images alone.

and Cl $2p_{3/2}$ at 55.8 and 198.5 eV are the same as the binding energies of these two ions in LiCl.[42]

It is also worth mentioning that, compared with the additive-free gypsum crystals, the Li^+ and Mg^{2+} surface adsorption via sulfate binding shifted the S $2p_{3/2}$ toward higher binding energies by 0.2 and 0.5 eV for Li^+ and Mg^{2+}, respectively (Figure S11). This shift was not observed for the adsorbed Na^+ or K^+, which indicates their low surface adsorption. Hou et al.[43] reported S $2p_{3/2}$ binding energy variations related to Mg^{2+} association with hydrothermally synthesized calcium sulfate hemihydrate crystals. They attributed this shift to the partial substitution of Ca^{2+} with Mg^{2+} in the calcium sulfate hemihydrate (bassanite) structure and the higher electronegativity of Mg^{2+} (1.39) with respect to Ca^{2+} (1.00), which explained the higher binding energy between Mg^{2+} and S compared to those between Ca^{2+} and S.

Analyzing the postdesorption gypsum crystals revealed that only Na^+ became partly (max 25%) incorporated into the gypsum structure. Such an incorporation likely happened through substitution of Na^+ for Ca^{2+}, specially as Na^+ has the closest ionic radius (1.16 Å) to Ca^{2+} (1.12 Å) compared to the other studied cations (Li^+ = 0.92 Å, K^+ = 1.52 Å, and Mg^{2+} = 0.89 Å). Therefore, in gypsum, it is likely that Ca^{2+} became substituted by 2 Na^+ ions with one of the Na^+ ions occupying the interstitial positions in the water layer.[1,44]

We are the first to show that, when gypsum crystals are grown in solutions containing low to high concentrations of monovalent and divalent ions, the prime interaction is through adsorption and that structural incorporation is only a minor effect for Na^+. Kushnir[45] reported that Sr^{2+}, Mg^{2+}, Na^+, and K^+ ions present in seawater brines became partitioned into growing gypsum crystals, but no determination whether the partitioning was because of the surface adsorption or structural incorporation is available. Recently, Wang and Meldrum[46] showed that gypsum crystals synthesized from experimental solutions containing 200 mM Mg^{2+} contained a small, but measurable, amount (0.4% mol) of Mg^{2+} in their structure. Similarly, Ben Ahmed et al.[17] suggested that a shift in *d*-spacing of the gypsum (020) peak indicates that Mg^{2+} became incorporated into the structure and suggested that this occurred by Mg^{2+} substituting for Ca^{2+}. On the basis of the same approach, they suggested that Na^+ did not incorporate into the

DOI: 10.1021/acs.cgd.6b01441
Cryst. Growth Des. 2017, 17, 582−589

gypsum structure. However, we clearly documented, by two complementary approaches (ICP-MS/ICP-OES analyses of pre- and postdesorption digests and XPS analyses of pre- and postdesorption crystal surfaces), that only less than 25% of Na^+ became incorporated into the gypsum structure, while all other ions, even at high concentrations, were solely adsorbed to the growing gypsum crystal surfaces. There, they affected both the growth kinetics and the shapes of the resulting gypsum crystals.

4.3. Morphological Modification. The selective adsorption of additives onto the growing gypsum crystals inhibited their growth along specific directions and thus modified their shapes (Figures 4 and S5). It is not surprising that such inhibition most often affects particular crystal faces as this depends on the attachment energies of each crystal face.[47] Recently, Massaro et al.[48] demonstrated theoretically that, for gypsum, there is a higher site density (Ca^{2+} and SO_4^{2-}) on the (021) faces compared to the fully hydrated (020) faces. Thus, it is likely that, because of the higher surface energy of the (021) face compared to the (020) face, adsorption will be more dominant on the (021) face. This is in line with our observations that adsorption preferentially occurred on the (021) faces and this led to an elongation in the *c* axis direction[49] (Figures 4, S5, and S12). In the presence of additives (specially Li^+ and Mg^{2+}), the resulting elongated gypsum crystals were accompanied by a corresponding decrease in the crystal widths (Figures 5 and S6). The observed spiral growth in the presence of additives, together with the uneven crystal tips and the presence of growth steps on the crystal surfaces (Figures 6 and S7–S10), suggests that indeed the additives played an important role in the growth of the gypsum crystals in our experiments. Such observations have not been reported before for mono- and divalent ions, but similar growth steps have been reported for gypsum crystals grown in the presence of acrylic polymers.[50] On the other hand, it is also well-known that any changes in supersaturation can have a distinct effect on growth morphology,[51,52] and this should be investigated in future studies.

5. CONCLUSION

With this study, we documented quantitatively the effects that alkali and alkaline earth metals have on the crystallization of gypsum. The additives increased the time needed for its precipitation to be initiated in the order of $K^+ < Na^+ < Li^+ < Mg^{2+}$. In all cases, gypsum was the sole precipitated phase after 200 min and the additives did not cause any phase transformation even at high salt concentrations. The combination of ICP-MS/ICP-OES of digested as-formed and postdesorbed digested gypsum crystals together with XPS analyses of the surfaces of these solids revealed that Li^+, K^+, and Mg^{2+} only adsorbed on the surfaces of the gypsum crystals, while a small fraction of associated Na^+ (max 25%) became structurally incorporated. Growing in the presence of all additives resulted in elongated gypsum crystals, with the change in aspect ratio compared to the additive-free system being most prominent in the presence of Li^+ and Mg^{2+} because of their higher surface adsorption affinities.

■ ASSOCIATED CONTENT

Supporting Information

The Supporting Information is available free of charge on the ACS Publications website at DOI: 10.1021/acs.cgd.6b01441.

Figures S1–S12 and Tables S1–S3 (PDF)

■ AUTHOR INFORMATION

Corresponding Authors

*E-mail: eetr@leeds.ac.uk (T.R.).
*E-mail: Benning@gfz-potsdam.de (L.G.B.).

ORCID

Taher Rabizadeh: 0000-0003-3483-2764

Funding

This work was funded by a European Commission Marie Initial Training Research network (Project number 290040) and by the German Helmholtz Recruiting Initiative.

Notes

The authors declare no competing financial interest.

■ ACKNOWLEDGMENTS

This study was supported by a Marie Curie grant from the European Commission in the framework of the MINSC ITN (Initial Training Research network), Project number 290040, and through the German Helmholtz Recruiting Initiative funding to L.G.B. and T.M.S. The authors would like to thank Stephen Reid and Dr. Andy Connelly from the Cohen Laboratories in the School of Earth and Environment for their support and Dr. Richard Walshaw at the Leeds Electron Microscopy and Spectroscopy Centre for help and access to instruments during the course of this study. We also thank two anonymous reviewers for their constructive comments.

■ REFERENCES

(1) Freyer, D.; Reck, G.; Bremer, M.; Voigt, W. *Monatsh. Chem.* **1999**, *130*, 1179–1193.
(2) Liu, H.; Bu, Y.; Nazari, A.; Sanjayan, J. G.; Shen, Z. *Constr. Build. Mater.* **2016**, *106*, 27–34.
(3) Ossorio, M.; Van Driessche, A. E. S.; Pérez, P.; García-Ruiz, J. M. *Chem. Geol.* **2014**, *386*, 16–21.
(4) Gupta, K.; Singh, S.; Rao, M. R. *Cryst. Growth Des.* **2016**, *16*, 3256–3261.
(5) Rahardianto, A.; Shih, W. Y.; Lee, R. W.; Cohen, Y. *J. Membr. Sci.* **2006**, *279*, 655–668.
(6) Van Driessche, A. E. S.; García-Ruiz, J. M.; Delgado-López, J. M.; Sazaki, G. *Cryst. Growth Des.* **2010**, *10*, 3909–3916.
(7) Hoang, T. A.; Ang, M.; Rohl, A. L. *Chem. Eng. Technol.* **2011**, *34*, 1003–1009.
(8) Akyol, E.; Öner, M.; Barouda, E.; Demadis, K. D. *Cryst. Growth Des.* **2009**, *9*, 5145–5154.
(9) Abdel-Aal, E.; Abdel-Ghafar, H.; El Anadouli, B. *Cryst. Growth Des.* **2015**, *15*, 5133–5137.
(10) Rabizadeh, T.; Peacock, C. L.; Benning, L. G. *Mineral. Mag.* **2014**, *78*, 1465–1472.
(11) Prisciandaro, M.; Olivieri, E.; Lancia, A.; Musmarra, D. *Ind. Eng. Chem. Res.* **2012**, *51*, 12844–12851.
(12) Hamdona, S. K.; Al Hadad, U. A. *J. Cryst. Growth* **2007**, *299*, 146–151.
(13) Sayan, P.; Titiz-Sargut, S.; Avcı, B. *Cryst. Res. Technol.* **2007**, *42*, 961–970.
(14) Kruger, A.; Focke, W. W.; Kwela, Z.; Fowles, R. *Ind. Eng. Chem. Res.* **2001**, *40*, 1364–1369.
(15) Morales, J.; Astilleros, J. M.; Matesanz, E.; Fernández-Díaz, L. *Minerals* **2016**, *6*, 22–35.
(16) Mao, X.; Song, X.; Lu, G.; Sun, Y.; Xu, Y.; Yu, J. *Ind. Eng. Chem. Res.* **2014**, *53*, 17625–17635.
(17) Ben Ahmed, S.; Tlili, M. M.; Amami, M.; Ben Amor, M. *Ind. Eng. Chem. Res.* **2014**, *53*, 9554–9560.
(18) Parkhurst, D. L.; Appelo, C. A. J. In *U.S. Geological Survey Techniques and Methods*; USGS: Reston, VA, 2013; Book 6, Chapter A43, p 497. http://pubs.usgs.gov/tm/06/a43/.

DOI: 10.1021/acs.cgd.6b01441
Cryst. Growth Des. 2017, 17, 582–589

(19) Aquilano, D.; Otálora, F.; Pastero, L.; García-Ruiz, J. M. *Prog. Cryst. Growth Charact. Mater.* **2016**, *62*, 227−251.
(20) Abràmoff, M. D.; Magalhães, P. J.; Ram, S. J. *Biophotonics Int.* **2004**, *11*, 36−41.
(21) Sun, J.; Wang, L.; Yu, G. *J. Chem. Eng. Data* **2015**, *60*, 2559−2566.
(22) Sverjensky, D.; Shock, E.; Helgeson, H. *Geochim. Cosmochim. Acta* **1997**, *61*, 1359−1412.
(23) Tanji, K. K. *Environ. Sci. Technol.* **1969**, *3*, 656−661.
(24) Zhang, Y.; Yang, Z.; Guo, D.; Geng, H.; Dong, C. *Procedia Environ. Sci.* **2013**, *18*, 84−91.
(25) Jiang, G.; Fu, H.; Savino, K.; Qian, J.; Wu, Z.; Guan, B. *Cryst. Growth Des.* **2013**, *13*, 5128−5134.
(26) Elgquist, B.; Wedborg, M. *Mar. Chem.* **1978**, *6*, 243−252.
(27) Reardon, E. *J. Phys. Chem.* **1975**, *79*, 422−425.
(28) Leaist, D. G.; Goldik, J. *J. Solution Chem.* **2001**, *30*, 103−118.
(29) Dove, P. M.; Czank, C. A. *Geochim. Cosmochim. Acta* **1995**, *59*, 1907−1915.
(30) Kerisit, S.; Parker, S. C. *J. Am. Chem. Soc.* **2004**, *126*, 10152−10161.
(31) Sakuma, H.; Kawamura, K. *Geochim. Cosmochim. Acta* **2011**, *75*, 63−81.
(32) Farmanesh, S.; Alamani, B. G.; Rimer, J. D. *Chem. Commun.* **2015**, *51*, 13964−13967.
(33) Kowacz, M.; Putnis, C.; Putnis, A. *Geochim. Cosmochim. Acta* **2007**, *71*, 5168−5179.
(34) Gierst, L.; Vandenberghen, L.; Nicolas, E.; Fraboni, A. *J. Electrochem. Soc.* **1966**, *113*, 1025−1036.
(35) Singh, N.; Middendorf, B. *Prog. Cryst. Growth Charact. Mater.* **2007**, *53*, 57−77.
(36) Bourikas, K.; Hiemstra, T.; Van Riemsdijk, W. *Langmuir* **2001**, *17*, 749−756.
(37) Johnson, S. B.; Scales, P. J.; Healy, T. W. *Langmuir* **1999**, *15*, 2836−2843.
(38) Sakuma, H.; Kawamura, K. *Geochim. Cosmochim. Acta* **2011**, *75*, 63−81.
(39) Rahnemaie, R.; Hiemstra, T.; van Riemsdijk, W. H. *J. Colloid Interface Sci.* **2006**, *293*, 312−321.
(40) Sobolewski, A. L.; Domcke, W. *Phys. Chem. Chem. Phys.* **2005**, *7*, 970−974.
(41) Siokou, A.; Kefalas, D.; Ntais, S. *Surf. Sci.* **2003**, *532*−*535*, 472−477.
(42) Naumkin, A. V.; Kraut-Vass, A.; Gaarenstroom, S. W.; Powell, C. J. *NIST X-ray Photoelectron Spectroscopy Database, Version 4.1*; National Institute of Standards and Technology: Gaithersburg, MD, 2012. http://srdata.nist.gov/xps/.
(43) Hou, S.; Wang, J.; Wang, X.; Chen, H.; Xiang, L. *Langmuir* **2014**, *30*, 9804−9810.
(44) Kushnir, J. *Geochim. Cosmochim. Acta* **1980**, *44*, 1471−1482.
(45) Kushnir, J. *Geochim. Cosmochim. Acta* **1982**, *46*, 433−446.
(46) Wang, Y. W.; Meldrum, F. C. *J. Mater. Chem.* **2012**, *22*, 22055−22062.
(47) Schmidt, C.; Ulrich, J. *J. Cryst. Growth* **2012**, *353*, 168−173.
(48) Massaro, F. R.; Rubbo, M.; Aquilano, D. *Cryst. Growth Des.* **2011**, *11*, 1607−1614.
(49) van der Voort, E.; Hartman, P. *J. Cryst. Growth* **1991**, *112*, 445−450.
(50) Montagnino, D.; Costa, E.; Massaro, F.; Artioli, G.; Aquilano, D. *Cryst. Res. Technol.* **2011**, *46*, 1010−1018.
(51) Yang, G.; Kubota, N.; Sha, Z.; Louhi-Kultanen, M.; Wang, J. *Cryst. Growth Des.* **2006**, *6*, 2799−2803.
(52) Prywer, J. *J. Cryst. Growth* **2006**, *289*, 630−638.

DOI: 10.1021/acs.cgd.6b01441
Cryst. Growth Des. 2017, 17, 582−589